

## The high-latitude artificial aurora of 21 February 1999: An analysis

M.J. Kosch<sup>1</sup>, M.T. Rietveld<sup>2</sup>, T.K. Yeoman<sup>3</sup>, K. Cierpka<sup>2</sup> and T. Hagfors<sup>2</sup>

<sup>1</sup>*Communication Systems, Lancaster University, Lancaster LA1 4YR, U.K.*

<sup>2</sup>*Max-Planck-Institut für Aeronomie, 37191 Katlenburg-Lindau, Germany*

<sup>3</sup>*Physics and Astronomy, Leicester University, Leicester LE1 7RH, U.K.*

**Abstract:** Artificial ionospheric optical emissions can be produced by high-power high-frequency (HF) radio waves. From the observation of HF induced artificial aurora on 21 February 1999, M.J. Kosch *et al.* (Geophys. Res. Lett., **27**, 2817, 2000) first noted the equatorward displacement of the optical emission towards the magnetic field line direction. This effect is investigated further and does not appear to be related to either the ion drift or neutral winds. HF coherent radar backscatter observations are presented for the first time in conjunction with artificial aurorae. Ray tracing suggests that the optical displacement may be related to the mechanism for producing field-aligned irregularities, which the radars require for receiving backscatter. The altitude of the artificial aurora has been estimated and is shown to be well below the reflection altitude and upper hybrid resonance height of the pump wave.

### 1. Introduction

High-power high-frequency (HF) radio waves can produce artificial optical emissions in the ionosphere due to electron bombardment of the neutrals. Optical observations are one of the few means of detecting energetic electrons produced from plasma turbulence generated by powerful HF waves in the ionosphere (*e.g.* Sipler and Biondi, 1972; Haslett and Megill, 1974; Bernhardt *et al.*, 1989a, b). The energisation threshold for the O(<sup>1</sup>D) 630 nm and the O(<sup>1</sup>S) 557.7 nm emissions is 1.96 eV and 4.17 eV, respectively (Bernhardt *et al.*, 1989a). However, the effective threshold to excite the O(<sup>1</sup>D) and O(<sup>1</sup>S) states is  $> 3.1$  and  $> 5.4$  eV, respectively, due to quenching by N<sub>2</sub> (Djuth *et al.*, 1999). Optical emissions at 630 nm have been observed at mid-latitude HF facilities such as Platteville (Haslett and Megill, 1974) and Arecibo (Sipler and Biondi, 1972; Gordon and Carlson, 1974; Bernhardt *et al.*, 1988), at Moscow (Adeishvili *et al.*, 1978) and the Sura facility near Vasilsurk (Bernhardt *et al.*, 1991). From mid-latitude studies, the optical emissions have been attributed to energetic electrons accelerated by Langmuir turbulence (Haslett and Megill, 1974; Sipler *et al.*, 1974; Weinstock, 1975; Gurevich *et al.*, 1985) as well as energetic electrons coming from the tail of a Maxwellian velocity distribution of HF enhanced electron temperature (Mantas, 1994; Mantas and Carlson, 1996; Gurevich and Milikh, 1997). Mishin *et al.* (2000) argue that the HF pumped electron energy distribution is not Maxwellian due to the interaction of N<sub>2</sub> regardless of the accelerating mechanism.

At auroral latitudes, an initial attempt to produce an artificial aurora (Stubbe *et al.*,

1982) was unsubstantiated by simultaneous independent observations (Henriksen *et al.*, 1984). The first unambiguous high-latitude artificial aurora observations of the O(<sup>1</sup>D) emission have been made more recently at Tromsø on 16 February 1999 (Brändström *et al.*, 1999) and 21 February 1999 (Kosch *et al.*, 2000a), using the EISCAT HF facility (Rietveld *et al.*, 1993) in northern Scandinavia, and on 18 March 1999 (Pedersen and Carlson, 2001) using the HAARP HF facility in Alaska. For the first observation, the high latitude artificial aurora is associated with very large electron temperature enhancements amounting to approximately 2500 K above background (Leyser *et al.*, 2000; Gustavsson *et al.*, 2001). Unfortunately, incoherent scatter measurements are unavailable for the other high-latitude artificial aurorae published to date. In this paper, we investigate all additional observations associated with the 21 February 1999 artificial aurora. This includes an altitude estimate of the optical emission, HF coherent radar and dynasonde backscatter, F-region ion drifts and neutral winds, and ray tracing of the pump wave.

## 2. Observations and discussion

On 21 February 1999, the EISCAT HF facility was operated in O-mode at 4.04 MHz with an effective radiated power of 73 MW in the vertical direction. The modulation was a sequence of 4-min on, 4-min off from 1648 to 1828 UT. A co-located advanced ionosonde (dynasonde) made soundings every 4 min from which the real reflection height of the pump wave was obtained using the true-height inversion program POLAN (Titheridge, 1967). The upper hybrid resonance height, which in our case is the height at which the plasma frequency is 240 kHz below the pump wave reflection height, was then computed. The directions of arrival and Doppler shifts of dynasonde backscatter were used to estimate F-region ion drift velocities (Wright and Pitteway, 1994). The CUTLASS pair of radars (Milan *et al.*, 1997), which are part of the SuperDARN network of similar radars (Greenwald *et al.*, 1995), recorded the artificial backscatter generated by HF O-mode pumping (Robinson *et al.*, 1997). In this study, CUTLASS used a 2-min beam scan with 45 km range resolution and operated at 12.4 MHz prior to 18 UT and at 10 MHz thereafter. However, only the Hankasalmi radar, which views predominantly poleward, received backscatter. The Digital All-Sky Imager (DASI) (Kosch *et al.*, 1998) was operated viewing in the zenith above Skibotn (69.35°N, 20.36°E), Norway, which is approximately 50 km south and east of the EISCAT HF facility (69.59°N, 19.23°E). Images were taken using a 116° field-of-view lens, a 630 nm narrowband interference filter and 10 s integration. A Fabry-Perot interferometer located at Skibotn (Kosch *et al.*, 1997) was used to estimate F-region neutral winds (Kosch *et al.*, 2000b). The instrument scans through north, south, east and west at 45° elevation as well as the vertical direction. Geomagnetic conditions were very quiet on 21 February 1999 with  $K_p=1$  during the period of interest, preceded by 9 hours of  $K_p=0^+$ .

A patch of artificial aurora started to appear  $\sim 10$  s after HF switch on, developing to a maximum peak intensity of about 100 Rayleighs above background within  $\sim 60$  s. When the HF pump was switched off the emission decayed within  $\sim 30$  s in agreement with the observations of Brändström *et al.* (1999). Pedersen and Carlson (2001) also found the rise time to be longer than the decay time. Panel A of Fig. 1 shows the time sequence of optical intensity, spatially averaged over the entire optical emission, in

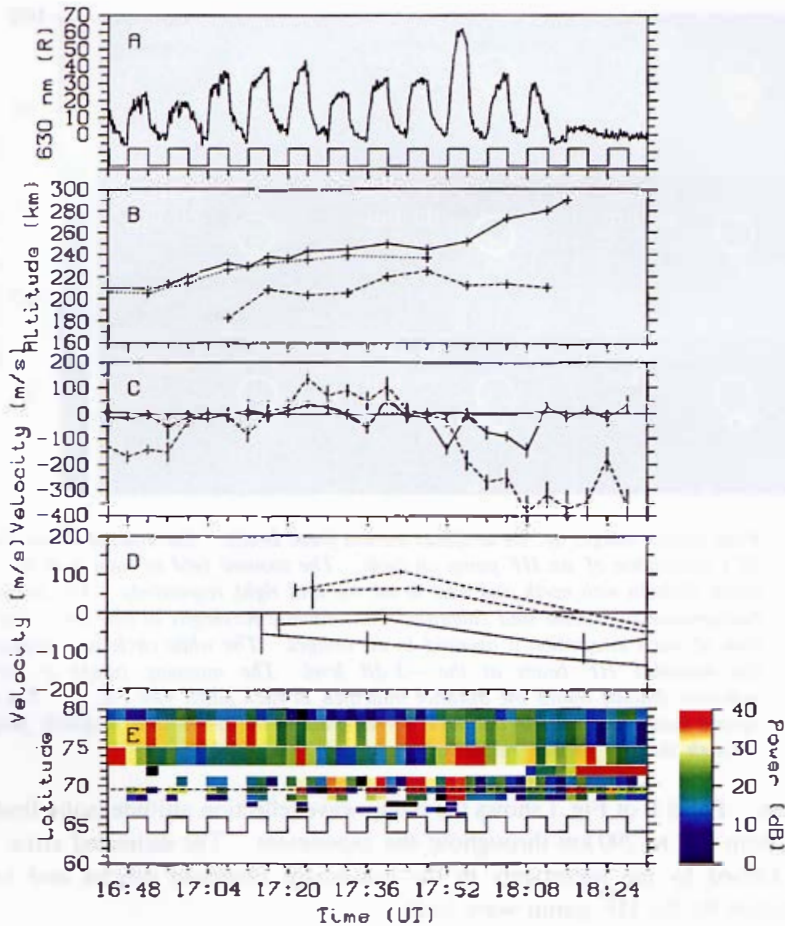


Fig. 1. An overview of the HF induced artificial aurora of 21 February 1999. Panel A shows the average intensity of the 630 nm emission above background. The square wave shows the HF pump on/off cycle. Panel B shows the 4.04 MHz O-mode reflection altitude (solid line), the upper hybrid resonance altitude (dotted line), and the height estimate of the optical emission (dashed line). Panel C shows meridional (solid line) and zonal (dashed line) f-region ion drifts over Tromsø. Panel D shows meridional (solid line) and zonal (dashed line) F-region neutral winds over Tromsø from opposite look directions. For panels C and D, positive is northward and eastward. Panel E shows a latitudinal keogram of HF coherent radar backscatter. The dashed line shows the location of the EISCAT HF facility.

Rayleighs for 630 nm. The data have been background subtracted, using images during no HF pumping, to remove scattered light from the setting sun. Negative intensities arise from noise in the background subtraction. The square wave represents the HF pump on/off cycle. In the interval 1648–1812 UT, there is a clear correlation between the transmitter being turned on (off) and the optical intensity rapidly increasing (decreasing). The data prior to 1704 UT is badly contaminated by a bright background sky and is not analysed further. The optical emission prior to 1648 UT is caused by phasing up of the HF

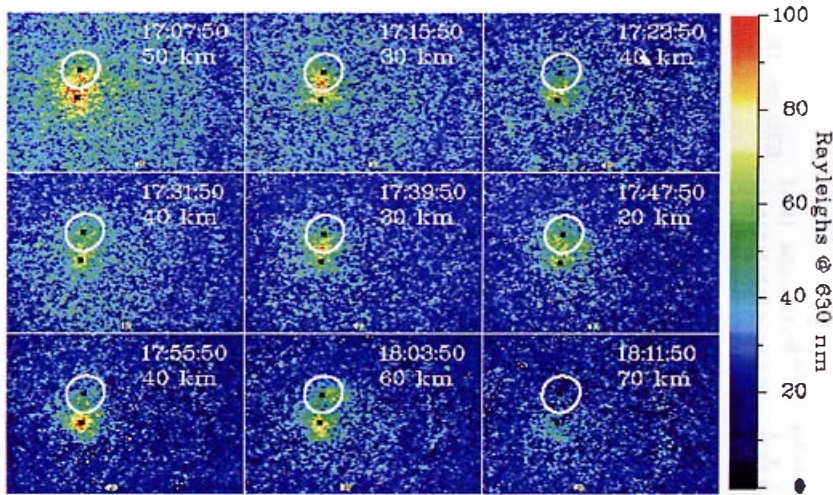


Fig. 2. False colour images of the artificial aurora from DASI. Each panel shows the last 10 s integration of an HF pump on cycle. The zoomed field of view is in the zenith above Skibotn with north and east to the top and right, respectively. The images are background subtracted and calibrated into absolute Rayleighs at 630 nm. The start time of each integration is overlaid in the images. The white circle is a mapping of the modelled HF beam at the  $-3$  dB level. The mapping height is the HF reflection altitude minus the distance indicated in each panel (see Fig. 1). The black square inside and outside the circle corresponds to the zenith and magnetic field line through the HF facility, respectively.

transmitters. Panel B of Fig. 1 shows the pump wave reflection altitude (solid line), which ascended from 210 to 290 km throughout the experiment. The estimated error is up to  $\pm 10$  km caused by the uncertainty in the trueheight inversion process and ionogram contamination by the HF pump wave itself.

Figure 2 shows a false-colour sequence of 9 DASI images taken 8 min apart, between 1704 and 1812 UT, each one being the last 10 s integration taken before the end of a 4-min HF on interval. North and east are to the top and right of each image, respectively, and the start time of each integration is overlaid in the images. The white circle shows the modelled HF beam for the  $-3$  dB locus. Assuming no refraction, the effective beam diameter corresponds to  $\sim 15^\circ$ , which is equivalent to a 65 km diameter at 250 km altitude. The black square outside the circle marks the intersection of the magnetic field line ( $12.8^\circ$  zenith angle at  $183.3^\circ$  azimuth) through the HF facility with the pump wave reflection height. The black square inside the circle marks the HF facility's location. A line joining both squares corresponds to the magnetic meridian direction over EISCAT.

Figure 2 is similar to Fig. 2 of Kosch *et al.* (2000a) where the HF beam  $-3$  dB locus was mapped to the pump wave reflection altitude. A clear equatorward shift of the optical emission compared to the HF beam projection was seen. In addition, these data showed a small but systematic westward shift of the optical emission compared to the projection of the HF beam, which is noted here for the first time. The westward displacement cannot be explained by refraction of the pump beam because the setting sun would ensure a descending electron density gradient from west to east, which would cause

an eastward refraction of the pump beam. Pedersen and Carlson (2001), whose optical imager was co-located with the HAARP HF facility, also observed the equatorward shift of the optical emission when pumping in the local zenith. However, most importantly, they found the optical emission to be exactly east-west symmetric across the magnetic meridian over the HF facility. This is confirmed by Gustavsson *et al.* (2001), in their Fig. 6, for 16 February 1999. Since DASI is not co-located with the EISCAT HF facility (50 km separation), and assuming geomagnetic east-west symmetry of the artificial aurora over EISCAT, it is possible to perform “one-legged” triangulation using the DASI images.

Figure 2 shows the HF beam mapped so that the optical emission is symmetrically located on the magnetic meridian over EISCAT. In order to achieve this, the projection altitude had to be reduced from the pump wave reflection altitude by the amount indicated in each image (20–70 km). Panel B of Fig. 1 shows the altitude of the artificial aurora (dashed line), which varied from 180 to 225 km  $\pm$  5 km. With the exception of the first data point at 1708 UT, the height of the artificial aurora remains remarkably constant (205–225 km) despite the steadily increasing pump wave reflection altitude. Using multi-station observations, Gustavsson *et al.* (2001) found the maximum optical emission to be 5–25 km below the pump wave reflection altitude. Model calculations by Bernhardt *et al.* (1989a) found the optical emission altitude to be  $\sim$ 0–25 km below the accelerated electron source region for HF interaction altitudes of 250–300 km. Mid-latitude altitude estimates by triangulation (Haslett and Megill, 1974) show that the optical emission was limited in height to  $280 \pm 15$  km although the pump wave reflection height could be up to 30 km higher. This is consistent with Bernhardt’s *et al.* (1989a) model. The direction of these results are also consistent with our observations, except that we estimate the vertical displacement to be somewhat greater with an average of  $\sim$ 40 km.

A potential problem with the accuracy of the “one-legged” altitude triangulation is indicated by comparing the radiative lifetime of the O(<sup>1</sup>D) emission with theoretical curves by Gustavsson *et al.* (2001). Their Fig. 8 shows that, for altitudes of 180–225 km, the radiative lifetime of O(<sup>1</sup>D) should be  $\sim$ 10–30 s. For 21 February 1999, the mean radiative lifetime is  $\sim$ 35 s. Ignoring the first altitude estimate (180 km), which may be contaminated by scattered sunlight, Gustavsson’s *et al.* (2001) theoretical estimate becomes  $\sim$ 15–30 s, which is still significantly less than that measured. Uncertainties in the “one-legged” altitude estimate includes errors in inverting the dynasonde data, mentioned earlier, and aligning the DASI images of the artificial aurora, which are noisy and diffuse, onto the EISCAT magnetic meridian. We conclude that our estimates probably constitute the lower bound for the altitude of the artificial aurora.

The large vertical displacement between the artificial aurora and the estimated pump wave reflection altitude is unexpected. If the mechanism of electron acceleration is Langmuir turbulence, then this would maximise at the pump wave reflection altitude. Leyser *et al.* (2000) suggested that upper hybrid turbulence could be a mechanism for electron acceleration. Panel B of Fig. 1 shows the estimated upper hybrid resonance (UHR) height (dotted line), which is 3–8 km below the pump wave reflection altitude. However, the optical emission is also well below the UHR height. It is possible that the energised electrons must travel to lower altitudes where the oxygen density is greater in order to produce an observable optical emission. This situation would be very similar to the natural aurora where the maximum brightness typically occurs near the bottom of the

auroral forms. In the case of the artificial aurora some evidence of vertical extent in the optical emission should be apparent (*e.g.* ray structures). To date, this is not apparent for both the 16 and 21 February 1999 data sets, where off axis optical recordings were made. Unfortunately, no electron temperature data are available for 21 February 1999. Gustavsson *et al.* (2001) show electron temperature altitude profiles for 16 February 1999. It seems clear that the electron temperature maximum is close to the pump wave reflection altitude (220–280 km) and temperature enhancements occur at all higher altitudes to beyond 500 km. Unfortunately, the 22 km range resolution makes it difficult to investigate the relationship between electron temperature and optical emission altitude as the artificial aurora appeared only 5–25 km below the pump wave reflection altitude on 16 February 1999. The same difficulty applies when comparing the electron temperature enhancements to the UHR height.

The artificial aurora shown in Fig. 2 is clearly equatorward of the projected pump beam. It should be noted that these images represent steady state conditions as each image is the last 10 s integration of a 4-min HF pump on cycle. Kosch *et al.* (2000a) showed that the displacement is not due to a geometric effect caused by the equatorward tilt of the magnetic field. Pedersen and Carlson (2001) suggested that the F-region ion drift might explain the displacement because the O(<sup>1</sup>D) photon is a forbidden transition and is only emitted ~110 s after energisation of O in free space. Panel C of Fig. 1 shows the F-region ion drift extracted from dynasonde data. The meridional and zonal components are shown as the solid and dashed lines, respectively, with error bars. North and east are defined as positive. For the period of interest, the meridional and zonal velocities are less than 150 and 400 m/s, respectively. During quiet geomagnetic conditions, which prevailed on 21 February 1999 ( $K_p=1$ ), the dynasonde produces accurate estimates of horizontal ion drift (Sedgemore *et al.*, 1998, and references therein). The velocities are consistent with CUTLASS radar Doppler shift data (not shown) (Eglitis *et al.*, 1998), which show the mainly meridional velocity to be less than 50 m/s. Gustavsson *et al.* (2001) have shown that the effective lifetime of O(<sup>1</sup>D) is less than 50 s below 250 km due to quenching by N<sub>2</sub>, O<sub>2</sub> and O. For the lowest measured altitude of the artificial aurora (180 km), the horizontal displacement between the zenith and magnetic field line directions is 40 km. For an O(<sup>1</sup>D) lifetime of 50 s and the maximum equatorward ion drift of 150 m/s, ion transport accounts for a possible maximum 7.5 km equatorward displacement. Using the maximum but less realistic lifetime of 110 s yields a maximum displacement of 16.5 km. Clearly, ion drift does not account for the displacement of the optical emission.

Pedersen and Carlson (2001) also suggested that the F-region neutral wind might explain the displacement of the artificial aurora. Panel D of Fig. 1 shows the thermospheric winds from Fabry-Perot interferometer measurements. The meridional and zonal components are shown as the solid and dashed lines, respectively, with error bars. North and east are defined as positive. The pairs of curves arise because any component of the neutral wind can be estimated twice by scanning the interferometer to opposite look directions. For the period of interest, the meridional and zonal velocities are less than 150 and 120 m/s, respectively. The same reasoning applies here as for the ion drifts. Hence, the neutral winds also cannot account for the displacement of the optical emission. This result is consistent with the observations of 16 February 1999 (Gustavsson *et al.*, 2001). We conclude that the displacement is probably an important clue to the mechanism of

artificial aurora generation at high latitudes. This conclusion is reinforced by the fact that the dynasonde sky plots, which show the direction of arrival of backscatter, often show a distinct equatorward displacement and appear to cluster around the magnetic field line direction. On 21 February 1999, dynasonde backscatter came from a region up to 100 km in diameter displaced  $\sim 50$  km equatorwards of zenith (not shown). This is entirely consistent with the displacement of the artificial aurora. The reason for this phenomenon remains unknown (J.W. Wright, private communication).

Bernhardt *et al.* (2000) found that the motion of the optical emission was a good indicator of F-region ion drift and neutral wind at low latitudes. Earlier we explained the small westward displacement of the artificial aurora from the magnetic meridian over the HF facility in terms of the reduced altitude of the optical emission. However, a westward ion drift would produce a similar displacement due to the long lifetime of O(<sup>1</sup>D). Kosch *et al.* (2000a) found no zonal drift motion of the optical emission for 21 February 2001. In addition, Fig. 2 in Kosch *et al.* (2000a) shows the westward displacement to always be present whereas Panels C and D of Fig. 1 shows the zonal ion drift and neutral wind, respectively, to be both eastward and westward at different times. We conclude that the altitude of the artificial aurora is below the pump wave reflection altitude and the westward displacement of the optical emission is not due to zonal ion drift or neutral wind. A future observation of artificial O(<sup>1</sup>S) aurora will provide definitive evidence as the lifetime of the 557.7 nm emission is only  $\sim 0.7$  s.

Panel E of Fig. 1 shows a latitudinal keogram of backscatter power from the CUTLASS (Hankasalmi) coherent radar. The square wave represents the HF pump on/off cycle. The dashed line shows EISCAT's location. The radar's over-the-horizon ray path has been corrected for refraction using the ionospheric electron density profile taken from the dynasonde. This results in a mapping accuracy of less than 1 range gate (45 km) (Yeoman *et al.*, 2001). There are clear and large enhancements in the backscatter power, up to 40 dB, during HF pump on periods centered on EISCAT's latitude. Natural backscatter exists poleward of EISCAT, which descends in latitude towards the end of the experiment.

Figure 3 shows the spatial extent of the CUTLASS coherent backscatter power for 15 HF pump on periods. The cross shows the location of the EISCAT HF facility. The central 9 panels correspond to the optical images shown in Fig. 2. The last 3 panels show the natural backscatter encroaching from the north. The area covered in each panel is  $400 \times 400$  km, whereas the artificial aurora has a diameter of  $\sim 50$  km. Hence, it is clear that the optical emission is very much more localised than the region of artificial backscatter. Coherent HF backscatter is produced by field-aligned irregularities (FAI), which are easily stimulated by HF O-mode pumping via resonant mode conversion to electrostatic waves (Robinson, 1989). Mode conversion occurs efficiently at the UHR height and artificial FAI are a common feature of HF O-mode pumping (Robinson *et al.*, 1998; Bond *et al.*, 1997). Electron temperature enhancements, as seen on 16 February 1999 (Leyser *et al.*, 2000), are also the final result of the conversion of HF waves into plasma waves and are correlated with FAI and anomalous absorption (Robinson *et al.*, 1997, 1998). Only about 5% of maximum pump power ( $\sim 10$  MW) is needed to produce FAI (Wright *et al.*, 2000) whereas the artificial aurora has proven difficult to stimulate even with maximum power. The spectral width of the CUTLASS backscatter (not shown) is less than 25 m/s,

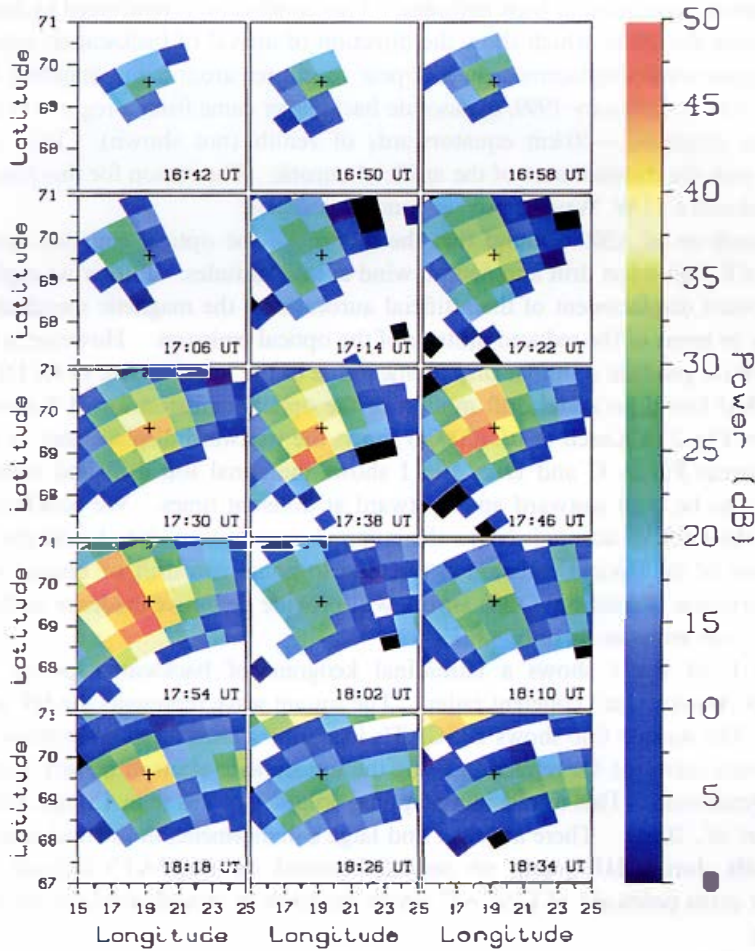


Fig. 3. Each panel shows the HF coherent backscatter power from the CUTLASS Hankasalmi radar in false colour centered over Tromsø. Each image corresponds to an HF pump on cycle. The central 9 panels correspond to the optical images shown in Fig. 2. The cross shows the location of the EISCAT HF facility.

which is relatively narrow. This is consistent with the pump wave enhanced FAI being an artificial hard target (Egilitis *et al.*, 1998).

Figure 4 shows the ray tracing diagram for a vertically directed 4.04 MHz  $\bullet$ -mode pump wave corresponding to the ionospheric conditions prevailing at 1732 UT on 21 February 1999 assuming a horizontally uniform ionosphere. The calculated ray paths are shown for incident angles to the zenith in  $3^\circ$  steps from  $15^\circ$  south to  $12^\circ$  north. The pump wave reflection altitude (dotted line) for 4.04 MHz is 244.9 km and the UHR height (dashed line) is 240.5 km. The orientation of the pump wave E-vector is shown by the arrows for the UHR height. The direction of the magnetic field line passing through the HF facility is shown by the dash-dotted line. The ionospheric electron density profile is shown by the dotted curve and relates to the upper  $x$ -axis, which is normalised to the pump

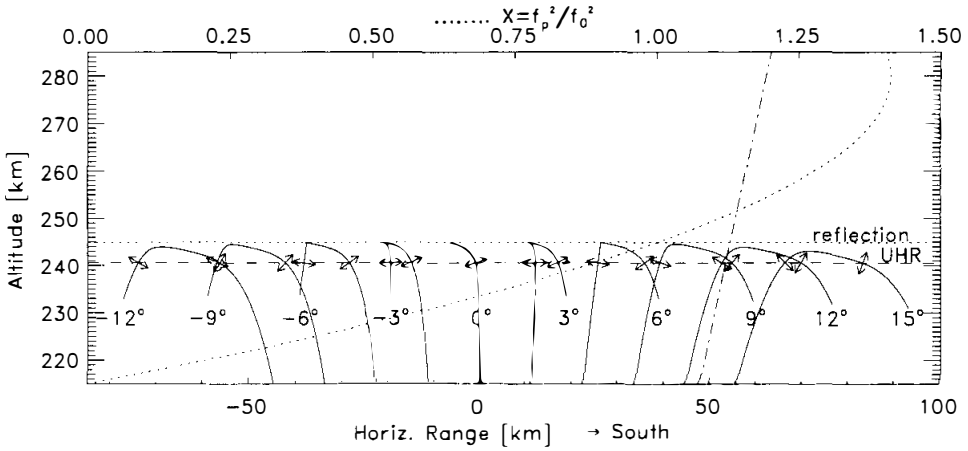


Fig. 4. A ray tracing diagram corresponding to the ionospheric conditions prevailing at 1732 UT on 21 February 1999 assuming a horizontally uniform ionosphere. The calculated ray paths are shown for a range of incident angles to the zenith. The HF reflection altitude (dotted line) is 244.9 km and the upper hybrid resonance height (dashed line) is 240.5 km. The orientation of the pump wave E-vector is shown by the arrows for the upper hybrid resonance height. The direction of the magnetic field line passing through the HF facility is shown by the dash-dotted line. The ionospheric electron density profile is shown by the curved dotted line and relates to the upper x-axis, which is normalised to the pump frequency of 4.04 MHz.

frequency of 4.04 MHz. The critical frequency was 4.8 MHz. All rays within the Spitzze cone ( $\pm 6^\circ$  at Tromsø) reach the maximum reflection altitude, as expected. By definition, the Spitzze angle is the critical zenith angle for which an O-mode wave still reflects at the maximum altitude (Rietveld *et al.*, 1993). For greater zenith angles the O-mode reflection altitude decreases, which is generally expected to reduce the occurrence of artificially stimulated plasma instabilities. Leyser *et al.* (2000) suggested that upper hybrid turbulence might be the mechanism for producing artificial aurora. Maximum coupling between the pump electromagnetic wave and upper hybrid electrostatic waves occurs when the pump wave electric field vector is perpendicular to the magnetic field line direction. This occurs at the UHR height approximately for the  $6^\circ$  southward ray upward leg and the  $9^\circ$  northward ray downward leg. We note that the  $6^\circ$  southward ray corresponds to the observed position of the artificial aurora. However, no optical emission is observed for the  $9^\circ$  northward ray position. This may be due to the fact that the northward ray has undergone reflection before meeting the condition for optimum coupling and will have lost strength due to absorption and conversion to other wave modes at reflection (*e.g.* Langmuir waves). In addition, the  $9^\circ$  northward ray is more than 3 dB weaker compared to the zenith (pump beam width  $\approx 15^\circ$ ). Hence, this ray is probably too weak to produce an observable optical emission. This reasoning will be tested in future by scanning the pump beam poleward.

The ray tracing and artificial aurora displacement are both consistent with the observed CUTLASS backscatter. The FAI, which coherent HF radars need for backscatter, are stimulated by electrostatic waves, which are most efficiently generated at the UHR

height where the pump wave electric field vector is perpendicular to the magnetic field. This condition is met for the ray path approximately  $6^\circ$  south of zenith. The large area of FAI produced by O-mode pumping is due to the fact that a significant component of the pump wave electric field vector is perpendicular to the magnetic field over a large area at the UHR height. The very much smaller area of the optical emission implies that only the most efficient coupling will produce an observable artificial aurora. The ray tracing, artificial aurora displacement and CUTLASS backscatter all provide evidence that the mechanism of electron acceleration, leading to the HF induced optical emission, may be linked to upper hybrid turbulence.

### 3. Conclusions

High-latitude HF induced artificial aurorae appear displaced equatorward towards the magnetic field line direction despite pumping in the local zenith. This effect was first noted on 21 February 1999 by Kosch *et al.* (2000a), was confirmed on 18 March 1999 (Pedersen and Carlson, 2001), and can be seen in the data from 16 February 1999 (Gustavsson *et al.*, 2001). On 21 February 1999, equatorward meridional F-region ion drifts and neutral winds do not exceed 150 m/s and hence cannot explain the displacement of the optical emission. Dynasonde backscatter also comes predominantly from the region where the optical emission is observed. The reason for this is unknown. Large HF coherent radar backscatter enhancements are associated with the production of artificial aurora. Ray tracing suggests that the optical displacement may be related to the mechanism for producing field-aligned irregularities, which the HF coherent radars require for receiving backscatter. This would be consistent with upper hybrid turbulence as a possible mechanism for the artificial aurora. However, details of the mechanism for particle acceleration, which is necessary for production of the optical emission, remain unclear. In addition, the altitude of the artificial aurora is shown to be well below the HF reflection altitude and upper hybrid resonance height of the pump wave.

### Acknowledgments

EISCAT is an international scientific association supported by the research councils of Finland, France, Germany, Japan, Norway, Sweden and the United Kingdom. The authors thank P. Gallop for implementing software by J.W. Wright for extracting ion drift velocities from dynasonde data, C. Davis for running the true-height inversion program and H. Kohl for the ray tracing program.

The editor thanks Drs. C. La Hoz and B. Gustavsson for their help in evaluating this paper.

### References

- Adeishvili, T.G., Gurevich, A.V., Lyakhov, S.B., Managadze, G.G., Milikh, G.M. and Shlyuger, I.S. (1978): Ionospheric emission caused by an intense radio wave. *Sov. J. Plasma Phys.*, **4**, 721-726.
- Bernhardt, P.A., Duncan, L.M., Tepley, C.A., Behnke, R.A. and Sheerin, J.P. (1988): Spatial and

- temporal evolution of 630.0 nm airglow enhancements during ionospheric heating experiments. *Adv. Space Res.*, **8**(1), 271-277.
- Bernhardt, P.A., Tepley, C.A. and Duncan, L.M. (1989a): Airglow Enhancements Associated With Plasma Cavities Formed During Ionospheric Heating Experiments. *J. Geophys. Res.*, **94**, 9071-9092.
- Bernhardt P.A., Duncan, L.M. and Tepley, C.A. (1989b): Heater-induced cavities as optical tracers of plasma drifts. *J. Geophys. Res.*, **94**, 7003-7010.
- Bernhardt, P.A., Scales, W.A., Grach, S.M., Karashtin, A.N., Kotik, D.S. and Polyakov, S.V. (1991): Excitation of artificial airglow by high power radio waves from the SURA ionospheric heating facility. *Geophys. Res. Lett.*, **18**, 1477-1480.
- Bernhardt, P.A., Wong, M., Huba, J.D., Fejer, B.G., Wagner, L.S., Goldstein, J.A., Selcher, C.A., Folov, V.L. and Sergeev, E.N. (2000): Optical remote sensing of the thermosphere with HF pumped artificial airglow. *J. Geophys. Res.*, **105**, 10657-10671.
- Bond, G.E., Robinson, T.R., Eglitis, P., Wright, D.M., Stocker, A.J., Rietveld, M.T. and Jones, T.B. (1997): Spatial observations by the CUTLASS coherent scatter radar of ionospheric modification by high power radio waves. *Ann. Geophys.*, **15**, 1412-1421.
- Brändström, B.U.E., Leyser, T.B., Steen, Å., Rietveld, M.T., Gustavsson, B., Aso, T. and Ejiri, M. (1999): Unambiguous evidence of HF pump-enhanced airglow at auroral latitudes. *Geophys. Res. Lett.*, **26**, 3561-3564.
- Djuth, F.T., Bernhardt, P.A., Tepley, C.A., Gardner, J.A., Kelley, M.C., Broadfoot, A.L., Kagan, L.M., Sulzer, M.P., Elder, J.H., Selcher, C., Isham, B., Brown, C. and Carlson, H.C. (1999): Large Airglow Enhancements Produced via Wave-Plasma Interactions in Sporadic E. *Geophys. Res. Lett.*, **26**, 1557-1560.
- Eglitis, P., Robinson, T.R., Rietveld, M.T., Wright, D.M. and Bond, G.E. (1998): The phase speed of artificial field-aligned irregularities observed by CUTLASS during HF modification of the auroral ionosphere. *J. Geophys. Res.*, **103**, 2253-2259.
- Gordon, W.E. and Carlson, H.C., Jr. (1974): Arecibo heating experiments. *Radio Sci.*, **9**, 1041-1047.
- Greenwald, R.A., Baker, K.B., Dudeney, J.R., Pinnock, M., Jones, T.B., Thomas, E.C., Villain, J.P., Cerisier, J.C., Senior, C., Hanuise, C., Hunsucker, R.D., Sofko, G., Koehler, J., Nielsen, E., Pellinen, R., Walker, A.D.M., Sato, N. and Yamagishi, H. (1995): DARN/SUPERDARN: A global view of the dynamics of high-latitude convection. *Space Sci. Rev.*, **71**, 761-796.
- Gurevich, A.V., Dimant, Ya. S., Milikh, G.M. and Vas'kov, V.V. (1985): Multiple acceleration of electrons in the regions of high-power radio-wave reflection in the ionosphere. *J. Atmos. Terr. Phys.*, **47**, 1057-1070.
- Gurevich, A.V. and Milikh, G.M. (1997): Artificial airglow due to modifications of the ionosphere by powerful radio waves. *J. Geophys. Res.*, **102**, 389-394.
- Gustavsson, B., Sergienko, T., Rietveld, M.T., Honary, F., Steen, Å., Brändström, B.U.E., Leyser, T.B., Aruliah, A.L., Aso, T., Ejiri, M. and Marple, S. (2001): First Tomographic estimate of volume distribution of HF-pump enhanced airglow emission. *J. Geophys. Res.*, **106**, 29105-29123.
- Haslett, J.C. and Megill, L.R. (1974): A model of the enhanced airglow excited by rf-radiation. *Radio Sci.*, **9**, 1005-1019.
- Henriksen, K., Stoffregen, W., Lybekk, B. and Steen, Å. (1984): Photometer and spectrometer search of the oxygen green and red lines during artificial ionospheric heating in the auroral zone. *Ann. Geophys.*, **2**, 73-76.
- Kosch, M.J., Hagfors, T. and Rees, D. (1997): A new Fabry-Perot interferometer for atmospheric studies with the EISCAT incoherent backscatter radar. *Adv. Space Res.*, **20**(6), 1133-1136.
- Kosch, M.J., Hagfors, T. and Nielsen, E. (1998): A new digital all-sky imager experiment for optical auroral studies in conjunction with the Scandinavian twin auroral radar experiment. *Rev. Sci. Instr.*, **69**(2), 578-584.
- Kosch, M.J., Rietveld, M.T. and Hagfors, T. (2000a): High-latitude HF-induced airglow displaced equatorwards of the pump beam. *Geophys. Res. Lett.*, **27**, 2817-2820.
- Kosch, M.J., Ishii, M., Nozawa, S., Rees, D., Cierpka, K., Kohsiek, A., Schlegel, K., Fujii, R., Hagfors,

- T., Fuller-Rowell, T.J. and Lathuillere, C. (2000b): A comparison of thermospheric winds and temperatures from Fabry-Perot interferometer and EISCAT radar measurements with models. *Adv. Space Res.*, **26**(6), 979-984.
- Leyser, T. B., Brändström, B.U.E., Gustavsson, B., Steen, Å., Honary, F., Rietveld, M.T., Aso, T. and Ejiri, M. (2000): Simultaneous measurements of high-frequency pump-enhanced airglow and ionospheric temperatures at auroral latitudes. *Adv. Polar Upper Atmos. Res.*, **14**, 1-11.
- Mantas, G.P. (1994): Large 6300-Å airglow enhancements observed in the ionosphere heating experiments based on analysis of Platteville, Colorado, data. *J. Geophys. Res.*, **99**, 8993-9002.
- Mantas, G.P. and Carlson, H.C. (1996): Reinterpretation of the 6300-Å airglow enhancements observed in ionosphere heating experiments based on analysis of Platteville, Colorado, data. *J. Geophys. Res.*, **101**, 195-209.
- Milan, S.E., Yeoman, T.K., Lester, M., Thomas, E.C. and Jones, T.B. (1997): Initial backscatter occurrence statistics from the CUTLASS HF radars. *Ann. Geophys.*, **15**, 703-718.
- Mishin, E., Carlson, H.C. and Hagfors, T. (2000): On the electron distribution function in the *F* region and airglow enhancements during HF modification experiments. *Geophys. Res. Lett.*, **27**, 2857-2860.
- Pedersen, T.R. and Carlson, H.C. (2001): First observations of HF heater-produced airglow at the High Frequency Active Auroral Research Program facility: Thermal excitation and spatial structuring. *Radio Sci.*, **36**, 1013-1026.
- Rietveld, M.T., Kohl, H., Kopka, H. and Stubbe, P. (1993): Introduction to ionospheric heating experiments at Tromsø, Part I: Experimental overview. *J. Atmos. Terr. Phys.*, **55**, 577-599.
- Robinson, T.R. (1989): The heating of the high latitude ionosphere by high power radio waves. *Physics Reports*, **179**, 79-209.
- Robinson, T.R., Stocker, A.J., Bond, G.E., Eglitis, P., Wright, D.M. and Jones, T.B. (1997): O- and X-mode heating effects observed simultaneously with the CUTLASS and EISCAT radars and low power HF diagnostics at Tromsø. *Ann. Geophys.*, **15**, 134-136.
- Robinson, T.R., Stocker, A., Bond, G., Eglitis, P., Wright, D., Jones, T.B. and Rietveld, M.T. (1998): First CUTLASS-EISCAT heating results. *Adv. Space Res.*, **21**(5), 663-666.
- Sedgemore, K.J.F., Wright, J.W., Williams, P.J.S., Jones, G.O.L. and Rietveld, M.T. (1998): Plasma drift estimates from the Dynasonde: comparison with EISCAT measurements. *Ann. Geophys.*, **16**, 1138-1143.
- Sipler, D.P. and Biondi, M.A. (1972): Measurements of O(<sup>4</sup>D) quenching rates in the *F* region. *J. Geophys. Res.*, **77**, 6202-6212.
- Sipler, D.P., Enemark, E. and Biondi, M.A. (1974): 6300-Å intensity variations produced by the Arecibo Ionospheric Modification Experiment. *J. Geophys. Res.*, **79**, 4276-4280.
- Stubbe, P., Kopka, H., Lauche, H., Rietveld, M.T., Brekke, A., Holt, O., Jones, T.B., Robinson, T., Hedberg, A., Thide, B., Crochet, B. and Lotz, H.J. (1982): Ionospheric modification experiments in northern Scandinavia. *J. Atmos. Terr. Phys.*, **44**, 1025-1041.
- Titheridge, J.E. (1967): The overlapping-polynomial analysis of ionograms. *Radio Sci.*, **2**, 1169-1175.
- Weinstock, J. (1975): Theory of enhanced airglow during ionospheric modifications. *J. Geophys. Res.*, **80**, 4331-4345.
- Wright, J.W. and Pitteway, M.L.V. (1994): High-resolution vector velocity determinations from the dynasonde. *J. Atmos. Terr. Phys.*, **56**, 961-977.
- Wright, D.M., Davies, J.A., Robinson, T.R., Chapman, P.J., Yeoman, T.K., Thomas, E.C., Lester, M., Cowley, S.W.H., Stocker, A.J., Horne, R.B. and Honary, F. (2000): Space Plasma Exploration by Active Radar (SPEAR): an overview of a future radar facility. *Ann. Geophys.*, **18**, 1248-1255.
- Yeoman, T.K., Wright, D.M., Stocker, A.J. and Jones, T.B. (2001): An evaluation of range accuracy in the SuperDARN over-the-horizon HF radar systems. *Radio Sci.*, **36**, 801-813.

*(Received December 18, 2001; Revised manuscript accepted April 30, 2002)*